

# Accuracy of Charge Densities in Electronic Structure Calculations

Moritz Gubler,<sup>1,\*</sup> Moritz R. Schäfer,<sup>2,3</sup> Jörg Behler,<sup>2,3</sup> and Stefan Goedecker<sup>1</sup>

<sup>1</sup>*Department of Physics, University of Basel, Klingelbergstrasse 82, CH-4056 Basel, Switzerland*

<sup>2</sup>*Lehrstuhl für Theoretische Chemie II, Ruhr-Universität Bochum, 44780 Bochum, Germany*

<sup>3</sup>*Research Center Chemical Sciences and Sustainability, Research Alliance Ruhr, 44780 Bochum, Germany*

Accurate charge densities are essential for reliable electronic structure calculations because they significantly impact predictions of various chemical properties and in particular, according to the Hellmann-Feynman theorem, atomic forces. This study examines the accuracy of charge densities obtained from different DFT exchange-correlation functionals in comparison with coupled cluster calculations with single and double excitations. We find that modern DFT functionals can provide highly accurate charge densities, particularly in case of meta-GGA and hybrid functionals. In connection with Gaussian basis sets, it is necessary to use the largest basis sets available to obtain densities that are nearly basis set error free. These findings highlight the importance of selecting appropriate computational methods for generating high-precision charge densities, which are for instance needed to generate reference data for training modern machine learned potentials.

## I. INTRODUCTION

Obtaining an accurate charge density is essential for predicting chemical properties, making it a cornerstone in quantum chemistry and materials science. The Hellmann-Feynman theorem [1] directly connects the accuracy of the charge density to the forces acting on the nuclei, emphasizing its importance for determining molecular geometries and molecular dynamics. Additionally, the Kohn-Sham theorems [2, 3], which form the basis of density functional theory (DFT), prove that the ground state electron density uniquely determines ground state properties. Beyond these theoretical principles, charge densities are modeled for example in charge equilibration schemes used in polarizable force fields, where the dynamic redistribution of charges is the key to determining molecular interactions, polarization effects, and reactivity in complex systems.

In recent years, machine learning potentials have become an important addition to *ab initio* methods, reproducing electronic structure calculations with high accuracy at only a fraction of the computational cost [4–11]. Many recent machine learning potentials [12–22] include effects like long range charge transfer, which necessitates the ability to accurately model charge densities using *ab initio* methods. Due to the high computational costs it is generally not feasible to compute reference data such as atomic Hirshfeld charges [23] using highly accurate methods like coupled cluster with single and double excitations (CCSD) [24, 25]. Instead, more approximate methods like DFT [2, 3] are typically used, trading some accuracy for increased computational efficiency. However, the accuracy of charge densities is strongly influenced by the choice of the exchange correlation functional and even the most accurate DFT functionals suffer from an electron self-interaction error [26–29] that impacts the accuracy of the charge density. Medvedev *et al.* [30] even claim that after the early 2000s the density error in DFT function-

als is in fact increasing. Controlling the self-interaction error in approximate forms of the exchange correlation functional is a highly active field of research, with many approaches aiming to remove this source of error [31–35].

In this paper, we benchmark widely distributed Gaussian basis sets in combination with various DFT functionals and compare the accuracy of the obtained charge densities with CCSD calculations using PySCF [36]. Specifically, we assess the performance of different basis sets, including polarization consistent [37] and correlation consistent [38] sets, and analyze the resulting densities in terms of the numerical stability of Hirshfeld charge partitioning.

By comparing the charge densities across various functionals and computational methods, we aim to identify the best strategies for obtaining high-precision and converged charge densities. Our findings have broad implications for computational chemistry, particularly in applications that require highly accurate modeling of electron density distributions such as modern machine learning potentials.

## II. METHODS

### A. Hirshfeld charges

The Hirshfeld charge [23]  $q_i$  of atom  $i$  is defined as

$$q_i = Z_i - \int \omega_i(\mathbf{r})\rho(\mathbf{r})d\mathbf{r} \quad (1)$$

where  $\omega_i(\mathbf{r}) = \frac{\rho_i(\mathbf{r})}{\sum_j \rho_j(\mathbf{r})}$  is the partitioning function of atom  $i$  and  $Z_i$  the atomic number of atom  $i$ . The atomic reference charge densities  $\rho_i(\mathbf{r})$  are spherically symmetric around atom  $i$  and are obtained and tabulated from free-atom calculations for each element in the system. Hirshfeld charges have the property that if  $\rho(\mathbf{r})$  is a superposition of the atomic reference charge densities then  $q_i = \int \rho_i(\mathbf{r})d\mathbf{r} = 0$ . Because of this property, Hirshfeld charges can be seen as a measure of the change of the

\* moritz.gubler@unibas.ch

charge density close to atom  $i$  compared to the reference charge density  $\rho_i$ .

Hirshfeld charges are typically used to analyze partial charges of atoms in molecules. However, there are some concerns that Hirshfeld charges are not well suited for this task since for example the dipole and quadrupole moments of the Hirshfeld charges differ significantly from the correct moments of the unpartitioned charge density [39], like those of many other partitioning methods. Hirshfeld charges can also be used to measure the dissimilarities of charge densities. In this work, one measure for the quality of a functional's charge density is the deviation of its Hirshfeld charges from those obtained using a CCSD reference. Hirshfeld charges are also used in several third- and fourth-generation machine learning potentials [12–14, 40] where they provide the reference data for modeling long range electrostatics and charge transfer.

In rare situations, the partitioning function  $\omega_i(\mathbf{r})$  may be numerically unstable since for points far away from all nuclei, both the numerator and the denominator are vanishing due to the exponential asymptotic decay of the charge density. However, in order to obtain accurate Hirshfeld charges, the partitioning function times the charge density must be integrated over the entire space. Numerical integration of Eq. (1) mandates the evaluation of the partitioning function in these critical regions.

Ratios of two very small quantities can be evaluated numerically in a numerically stable way with the log-sum-exp-trick. The log-sum-exp (LSE) operation is defined as  $\text{LSE}(x_1, \dots, x_n) = \ln(\sum_{i=1}^n \exp(x_i))$ . By shifting all components with  $x^* = \max\{x_1, \dots, x_n\}$ , the LSE can be evaluated accurately even if the range of  $x_i$  is large:  $\text{LSE}(x_1, \dots, x_n) = x^* + \ln(\sum_{i=1}^n \exp(x_i - x^*))$ . Let  $\tilde{\rho}_i(\mathbf{r}) = \ln(\rho_i(\mathbf{r}))$ . Using the numerically stable LSE function, the partitioning function can be rewritten as

$$\omega_i(\mathbf{r}) = \exp(\tilde{\rho}_i - \text{LSE}(\tilde{\rho}_1(\mathbf{r}), \dots, \tilde{\rho}_n(\mathbf{r}))). \quad (2)$$

The expression in Eq. (2) is numerically stable for all values of  $\rho_i(\mathbf{r})$ . We implemented this in PySCF [36] and the multi wavelet based software MRChem [41, 42].

## B. Gaussian basis sets

The spherical symmetry of the nuclear potential motivates the following ansatz for a basis function centered on atom  $\alpha$ :  $\exp(-a_k \|\mathbf{r} - \mathbf{r}_\alpha\|^2) \cdot Y_{lm}(\theta_\alpha, \varphi_\alpha)$  where  $\|\mathbf{r} - \mathbf{r}_\alpha\|$  is the distance to atom  $\alpha$ ,  $\theta_\alpha$ ,  $\varphi_\alpha$  are the polar and azimuthal angle of  $\mathbf{r} - \mathbf{r}_\alpha$  respectively,  $Y_{lm}(\theta_\alpha, \varphi_\alpha)$  is a spherical harmonic function and the parameter  $a_k$  controls the width of the Gaussian basis function. Orbitals can then be expressed as linear combinations of these basis functions.

In Gaussian basis sets, the coefficients  $a_k$  and the number of spherical harmonic functions  $Y_{lm}$  are chosen for

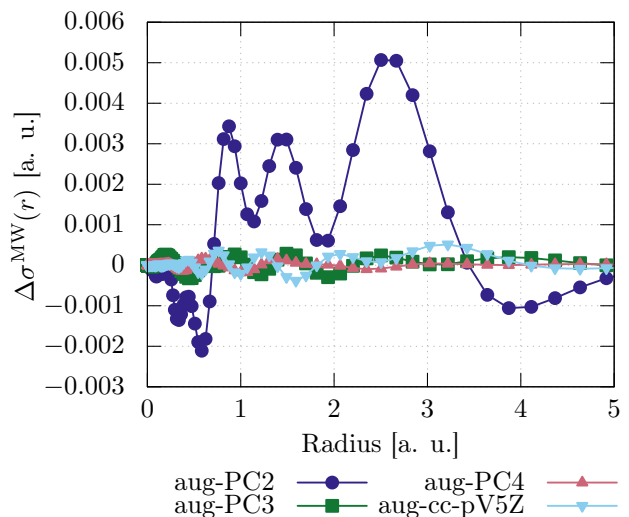


FIG. 1. Basis set error  $\Delta\sigma^{\text{MW}}$  of DFT charge densities using the PBE functional for various DFT optimized, polarization consistent (PC) basis sets for a neon atom. A multi wavelet (MW) charge density is used as the reference value.

each element by fitting these coefficients to reference values that are obtained analytically or with a more accurate basis set.

The biggest advantage of Gaussian orbitals is that overlap, kinetic, nuclear repulsion and coulomb integrals can be solved analytically.

Disadvantages of Gaussian basis sets are that a large number of Gaussian functions is required to accurately represent the nuclear cusps in wave functions and Gaussian basis sets are not orthonormal meaning that convergence of the basis set to the complete basis set limit can not necessarily be achieved by adding more basis functions. Finally, the condition number of the overlap matrix increases with the addition of Gaussian basis functions, leading to numerical problems that often limit the number of basis functions that can be used in a calculation.

## C. Multi resolution Wavelets

Multi wavelets [43, 44] provide a robust framework for representing quantum mechanical orbitals by utilizing adaptive grids and rigorous error control. They form a systematic basis, which means that by adding more and more basis functions an arbitrarily high accuracy can be achieved without running into numerical instabilities. Unlike scalar wavelets, which rely on a single basis function per grid interval, multi wavelets use multiple basis functions inside each grid interval.

When a function is represented using multi wavelets, all quantities are mapped on an adaptive grid. Inside each grid interval multiple Legendre polynomials are used to represent the desired function. These Legendre polynomials are confined strictly within each grid element and

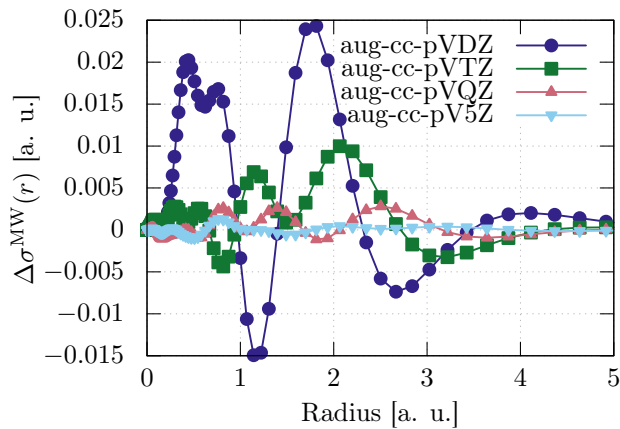


FIG. 2. Basis set error  $\Delta\sigma$  of DFT charge densities using the PBE functional for correlation consistent basis sets for a neon atom. A multi wavelet charge density is used as the reference value.

are truncated at the edges resulting in discontinuities of the wavefunctions and other quantities at the borders of neighboring grid intervals. The fact that the truncation removes all overlap between multi wavelets across different grid intervals enables the efficient implementation of adaptive grids. The discontinuities between grid intervals do not impact the precision of integral calculations, which is why an integral based formulation has to be used when solving the Kohn–Sham equations in a multi-wavelet basis [45, 46].

The adaptivity of multi wavelets allows to perform all-electron calculations where the resolution is increased for rapidly varying core orbitals, focusing computational resources where needed. Rigorous error control within multi wavelet methods enables the user to define the desired precision before the calculation begins, ensuring that the basis set error remains smaller than the chosen precision. For low precision wavelet calculations are generally slower than those using Gaussian orbitals, but when a large number of Gaussians is employed to obtain high precision, their efficiency becomes comparable. These features make multi wavelets particularly well suited for reference calculations in quantum mechanical applications, where both accuracy and efficiency are essential.

The Multi wavelet approach can be coupled by a separable form to represent Greens functions of the Poisson and Helmholtz equation [47] which enables efficient Hartree Fock [46] and DFT [45] calculations.

These features are implemented in the software package MRChem [41, 42] and this code will be used for all wavelet based calculations in this paper.

### III. RESULTS

#### A. Basis set errors of charge densities

Before comparing charge densities obtained with different exchange correlation functionals, it is essential to assess the density error resulting from the Gaussian basis functions. To do this, the basis set errors of DFT using the PBE functional [48] are compared against basis-set-error-free charge densities obtained from a MRChem [41] multi wavelet calculation.

A single neon atom was chosen as a test system since its charge density is spherically symmetric which simplifies visualization and comparison of charge densities. In this context, a useful quantity is

$$\sigma(r) = \int_{r=0}^r \int_{\phi=0}^{2\pi} \int_{\theta=0}^{\pi} \rho(r', \theta, \phi) r'^2 \sin \theta dr' d\phi d\theta, \quad (3)$$

which is a one dimensional function  $\sigma(r)$  that contains the charge inside a sphere of radius  $r$ . When spherically symmetric charge densities are considered, no information about the three dimensional charge density is lost. When comparing the charge density obtained with a DFT functional and a CCSD charge density, plotting the difference in  $\sigma$  offers insights into the spatial error distribution of the charge density. The difference in  $\sigma$  between two methods has units of charge and is the difference of charge contained in a sphere with radius  $r$ . It is called  $\Delta\sigma^{\text{CC}}$  when a DFT charge density is compared to CCSD results and  $\Delta\sigma^{\text{MW}}$  when a DFT charge density that was obtained using a Gaussian basis set is compared with a multi wavelet calculation in this paper.

First, the error of the charge density for polarization consistent Gaussian basis sets [37] that are optimized for DFT calculations is analyzed. In Fig. 1, the difference of  $\sigma$  between an basis-set-error-free multi wavelet charge density and a charge density obtained with polarization consistent basis sets [37] is shown. The charge density was calculated with the PBE functional for a single neon atom. The “aug” prefix indicates the addition of diffuse functions in the Gaussian basis set. The aug-PC3 and aug-PC4 basis sets agree well with the multi wavelet reference calculation. For comparison, a charge density that was obtained using a correlation consistent basis set (aug-cc-pV5Z) is added in Fig. 1 which gives the same level of accuracy in the charge density. The aug-PC3 contains fewer basis functions than the aug-cc-pV5Z basis set, the aug-PC4 more. In Fig. 2 the basis set error of charge densities obtained with a correlation consistent basis [38] sets is shown. Also the aug-cc-pV5Z basis set matches the multi wavelet result almost perfectly. It is therefore recommended to use this basis set whenever highly accurate charge densities are necessary with wave function based methods. The aug-PC3 and aug-PC4 offer the same level with a similar number of basis functions, the aug-PC3 is even a bit smaller than the aug-cc-pV5Z and is therefore an interesting alternative to the correlation consistent basis set when DFT is used. In Fig. 3

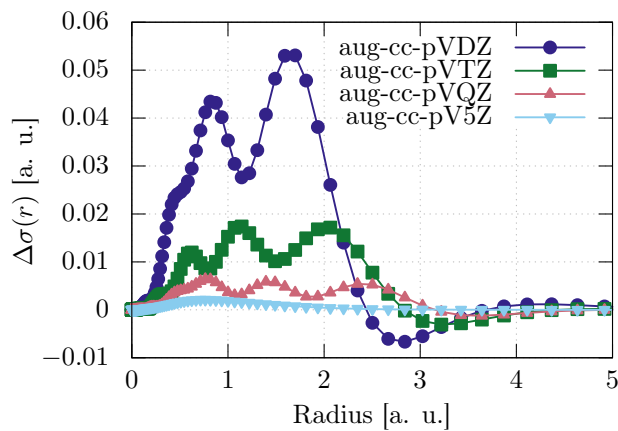


FIG. 3. Basis set error  $\Delta\sigma$  of CCSD charge densities with respect to the basis set. A calculation with a aug-cc-pwPV5Z was used as the reference charge density.

it is shown that the aug-cc-pV5Z basis set also produces highly accurate charge densities for coupled cluster calculations with single and double excitations. The error of charge densities with the cc-pVNZ and the PC basis is analyzed in Fig. 4 for a methanol molecule. The reference charge density was obtained using a multi wavelet DFT calculation with the PBE functional. As a measure of error, in this case the absolute value of the difference in Hirshfeld charges is used. Here, the addition of diffuse Gaussian basis functions greatly improves the accuracy and once again, the aug-cc-pV5Z basis is able to produce highly accurate charge densities. The aug-PC3 and aug-PC4 basis sets also produce highly accurate Hirshfeld charges, the aug-PC4 appears to be the most accurate basis set in this comparison. However, the calculation using the aug-PC4 basis set was difficult to converge since the condition number of the overlap matrix from the basis functions was larger than  $10^8$ . aug-PC3, aug-PC4 and the aug-cc-pV5Z offer sufficient precision to accurately compare charge densities obtained with different functionals. Given that DFT results are being compared to CCSD calculations, it is more consistent to use the correlation-consistent aug-cc-pV5Z basis set, which is specifically designed for post-Hartree-Fock methods. Therefore, in the remainder of this paper, the aug-cc-pV5Z basis set will be used for comparing various exchange-correlation functionals.

### B. Accuracy measures of charge densities

Having found a suitable basis set to calculate high-precision charge densities, the charge densities for a variety of different exchange correlation functionals can be compared with accurate coupled cluster calculations with single and double excitations (CCSD). PySCF [36] was used for the CCSD calculations and the DFT calculation employing Gaussian basis sets. The charge densities of

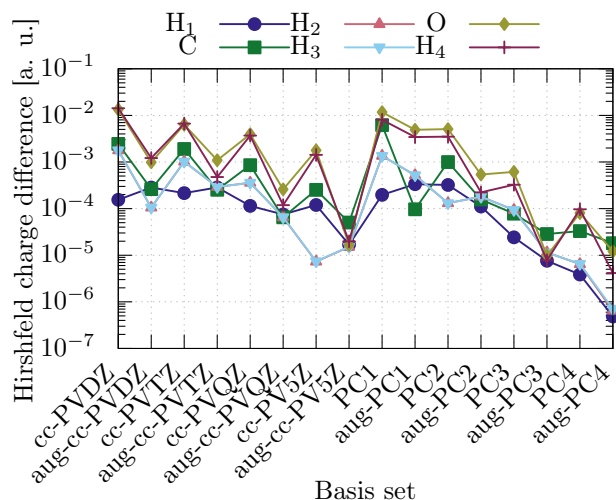


FIG. 4. Basis set errors of Hirshfeld charges for different Gaussian basis sets for the atoms of a methanol molecule. Reference values were obtained using a multi wavelet calculation using the MRCHEM code. The same spherically symmetric reference charge densities were used to compute the Hirshfeld charges in all the different codes.

twelve different DFT functionals and Hartree Fock are benchmarked against CCSD charge densities for several molecules that are small enough to allow a CCSD calculation with an aug-cc-pV5Z basis set. The molecules are:

AlH <sub>3</sub>	Ar	BeH <sub>2</sub>	BH <sub>3</sub>	CH <sub>4</sub>	F <sub>2</sub>
H <sub>2</sub>	H <sub>2</sub> O	H <sub>2</sub> S	HCl	He	HF
LiH	Li <sub>2</sub>	MgH <sub>2</sub>	N <sub>2</sub>	NaH	Ne
NH <sub>3</sub>	PH <sub>3</sub>	SiH <sub>4</sub>	CH <sub>2</sub> O	CO <sub>2</sub>	CO
H <sub>2</sub> O <sub>2</sub>	HCN				

For these molecules, six different measures of error with respect to the reference CCSD charge densities are calculated:

1. Root mean squared error (RMSE) of the Hirshfeld charges
2. Average absolute value of maximal point wise charge difference.
3. The average integral over  $(\rho - \rho_{\text{CCSD}})^2$
4. Average Coulomb energy of  $\rho - \rho_{\text{CCSD}}$ . This attenuates the short wavelength component of  $(\rho - \rho_{\text{CCSD}})^2$ .
5. Average infinity norm of difference in dipole moments
6. Average infinity norm of difference in quadrupole moments

The integrals required to calculate the norms were evaluated numerically with the integration grids of PySCF



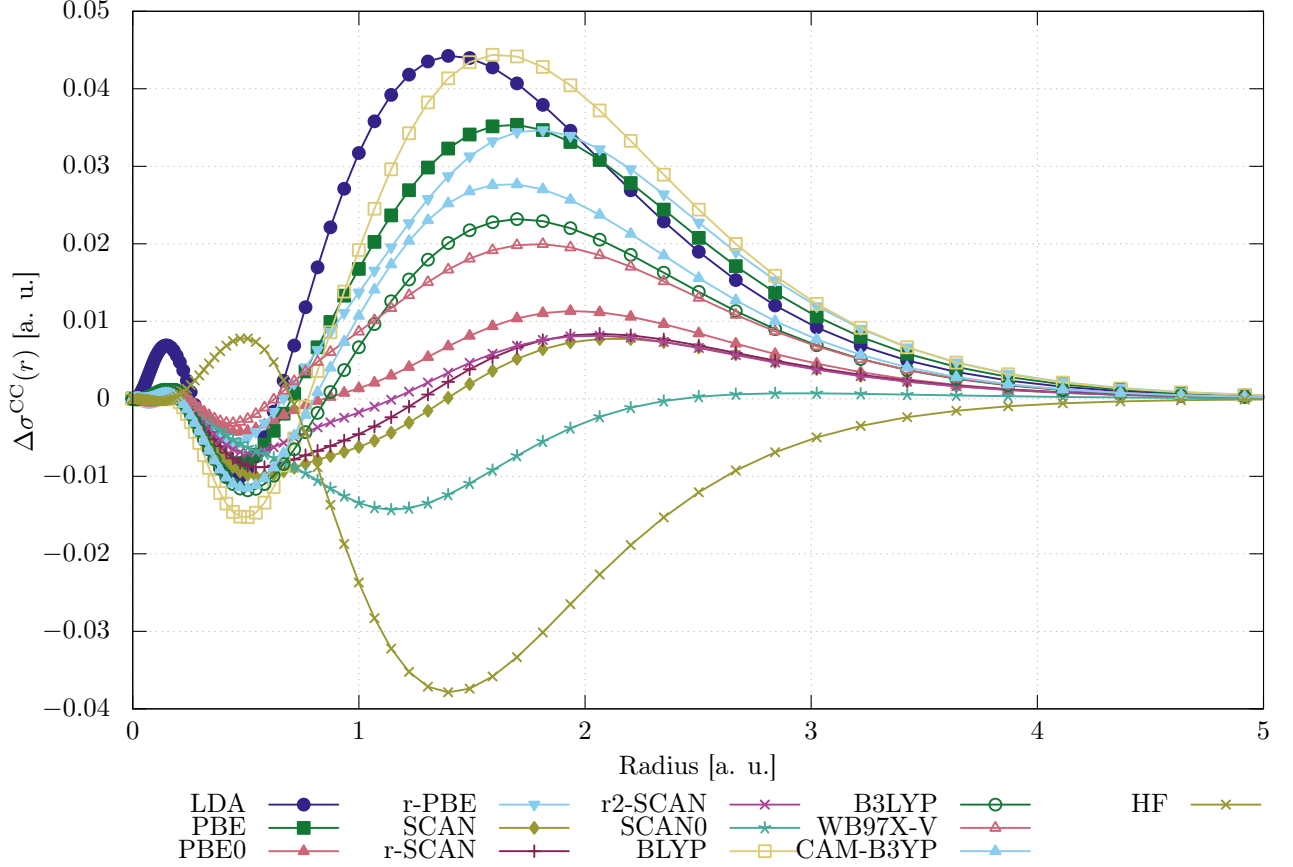


FIG. 5. The difference in  $\sigma(r)$  for CCSD charge densities and various DFT functionals of a neon atom. Negative values mean that the charge density of a functional contains more electrons than the CCSD reference calculation for a given radius.

using the accurate grid level. The reference charge densities required for the calculation of the Hirshfeld charges were taken from Abinit [49]. In Fig. 6, these measures are shown for all functionals. The functionals tested are:

1. LDA with Slater exchange [50] and VWN correlation [51]
2. PBE [48]
3. r-PBE [52]
4. Becke exchange [53] and LYP correlation [54] (BLYP)
5. B3LYP [53, 55–57]
6. PBE0 [58, 59]
7. SCAN [60]
8. r-SCAN [61]
9. r2-SCAN [62]
10. SCAN0 [63]
11. CAM-B3LYP [64]
12. WB97X-V [65, 66]

### C. Accuracy of different exchange correlation functionals

We now analyse the accuracy of the different exchange correlation functionals for the investigated set of small molecules. Our previously defined measures of accuracy of the charge densities can be divided in two categories: point-wise measures and integral-based measures. The only point-wise measure used is the average maximal difference in charge density. The maximal difference in charge density is always located at the nuclear cusps. In this point-wise comparison, the Hartree Fock charge density most accurately approximates the CCSD charge density. The LDA charge density is worst regarding the point-wise measure and there is no clear trend in the remaining DFT functionals.

However, the situation changes when considering the integral-based measures. In this case, HF and LDA yield poor charge densities, while all other functionals show significantly higher accuracy. The PBE, rPBE, and the BLYP functional are able to reproduce CCSD charge densities accurately in most tests but they struggle to accurately predict good dipole and quadrupole moments. The functionals that consistently produce good charge

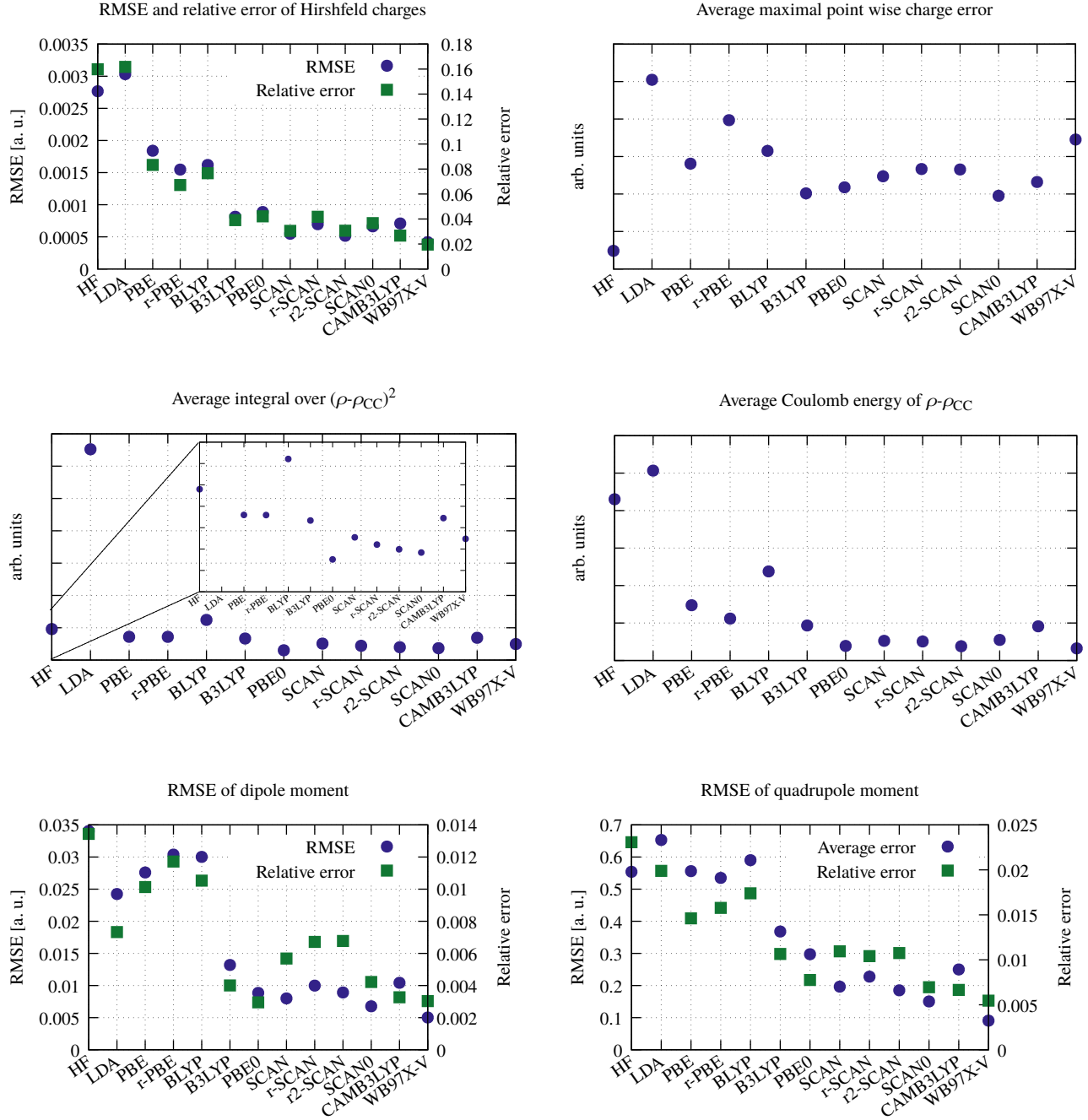


FIG. 6. Average errors of all measures for the quality of charge densities for a series of benchmark molecules. The calculations were done with the Gaussian aug-cc-pV5Z basis set and the PySCF code. CCSD charge densities were used as reference charge densities to compute the error of a given method.

densities all either hybrid or meta-GGA. There is no clear benefit in the usage of range-separated hybrid functionals compared to modern state-of-the-art meta-GGA functionals such as r2-SCAN. The accuracy in the charge densities is similar in meta-GGA and hybrid functionals, making meta-GGA functionals the optimal choice that balance accuracy in charge densities and computational

cost. Moreover, exact exchange is not needed to compute accurate Hirshfeld charges. The SCAN, r-SCAN and r2-SCAN functionals produce highly accurate Hirshfeld charges with an average relative error of around 4 percent making them ideal methods to compute reference data for machine learning potentials. B3LYP, PBE0, SCAN0 and the range-separated hybrid functionals CAM-B3LYP

and WB97X-V are similarly accurate. Since they all contain exact exchange they are computationally significantly more expensive.

Very similar trends are found when analysing a single atom. In Fig. 5, the difference in  $\sigma(r)$  is shown for the tested functionals. It is found that r2-SCAN, SCAN and SCAN0 have the smallest error closely followed by PBE0, B3LYP and the range-separated hybrid functional WB97X-V.

#### IV. CONCLUSION

A thorough investigation of the charge density error of Gaussian basis sets revealed that a very large basis set is required to accurately model the charge density. Polarization consistent basis sets that have been originally optimized for DFT calculations contain lower angular momenta in the Gaussian basis sets compared to the correlation consistent basis sets optimized for post-Hartree Fock calculations. The aug-cc-pV5Z, aug-PC3 and aug-PC4 basis sets are able to obtain accurate DFT charge densities making them the optimal choice for situations where highly accurate charge densities are needed. When molecular systems are considered, adding diffuse basis functions greatly improves the accuracy of the charge density. The aug-cc-pV5Z basis set appears to be accurate enough to obtain good charge densities. Our results are also of interest in the context of constructing machine learned potentials whose atomic charges are fitted to density functional results [12]. Since the atomic Hirshfeld charges obtained by different exchange correlation functionals differ by a few percent, there is no point trying to fit them in machine learning schemes to much higher precision.

An analysis of various metrics assessing the charge density quality showed that modern DFT functionals outperform Hartree-Fock for simple molecules. In these cases,

density corrected DFT calculations [67] will therefore not improve the accuracy. The only functional that performs worse than HF is LDA. In contrast, all GGA, meta-GGA, and hybrid functionals evaluated in this study yield more accurate charge densities than HF. This trend suggests that the modern variants of meta-GGA and hybrid functionals are continuously enhancing the accuracy of charge densities in electronic structure calculations. The sole measure where HF excels is the maximal point-wise error in the charge density, which consistently occurs at the nuclear positions.

#### V. CODE AVAILABILITY

A modified copy of MRCHEM that allows the calculation of Hirshfeld charges can be found in the GitHub repository: <https://github.com/moritzgubler/mrchem/tree/property/hirshfeld>. A python library was developed to analyze and compare DFT and CCSD charge densities using the PySCF [36] framework. This library can be found here: <https://github.com/moritzgubler/charge-partitioning>

#### ACKNOWLEDGMENTS

Financial support was obtained from the Swiss National Science Foundation (project 200021 191994) and the Deutsche Forschungsgemeinschaft (DFG, German Research Foundation, project 495842446) in the framework of the DFG priority program SPP 2363. The calculations were performed on the computational resources of the Swiss National Supercomputer (CSCS) under project s1167 and on the Scicore (<http://scicore.unibas.ch/>) computing center of the University of Basel.

- 
- [1] R. P. Feynman, *Phys. Rev.* **56**, 340 (1939).
  - [2] P. Hohenberg and W. Kohn, *Phys. Rev.* **136**, B864 (1964).
  - [3] W. Kohn and L. J. Sham, *Phys. Rev.* **140**, A1133 (1965).
  - [4] J. Behler, *J. Chem. Phys.* **145**, 170901 (2016).
  - [5] V. L. Deringer, M. A. Caro, and G. Csányi, *Adv. Mater.* **31**, 1902765 (2019).
  - [6] F. Noé, A. Tkatchenko, K.-R. Müller, and C. Clementi, *Ann. Rev. Phys. Chem.* **71**, 361 (2020).
  - [7] O. T. Unke, S. Chmiela, H. E. Sauceda, M. Gastegger, I. Poltavsky, K. T. Schütt, A. Tkatchenko, and K.-R. Müller, *Chem. Rev.* **121**, 10142 (2021).
  - [8] J. Behler and G. Csányi, *Eur. Phys. J. B* **94**, 142 (2021).
  - [9] E. Kocer, T. W. Ko, and J. Behler, *Ann. Rev. Phys. Chem.* **73**, 163 (2022).
  - [10] P. Friederich, F. Häse, J. Proppe, and A. Aspuru-Guzik, *Nat. Mater.* **20**, 750 (2021).
  - [11] K. T. Schütt, H. E. Sauceda, P.-J. Kindermans, A. Tkatchenko, and K.-R. Müller, *J. Chem. Phys.* **148**, 241722 (2018).
  - [12] T. W. Ko, J. A. Finkler, S. Goedecker, and J. Behler, *Nature Communications* **12**, 398 (2021).
  - [13] M. Gubler, J. A. Finkler, M. R. Schäfer, J. Behler, and S. Goedecker, *Journal of Chemical Theory and Computation* **20**, 7264 (2024), pMID: 39151921.
  - [14] S. A. Ghasemi, A. Hofstetter, S. Saha, and S. Goedecker, *Phys. Rev. B* **92**, 045131 (2015).
  - [15] S. Faraji, S. A. Ghasemi, S. Rostami, R. Rasoulkhani, B. Schaefer, S. Goedecker, and M. Amsler, *Phys. Rev. B* **95**, 104105 (2017).
  - [16] E. R. Khajepasha, J. A. Finkler, T. D. Kühne, and S. A. Ghasemi, *Phys. Rev. B* **105**, 144106 (2022).
  - [17] R. Zubatyuk, J. S. Smith, B. T. Nebgen, S. Tretiak, and O. Isayev, *Nature Communications* **12**, 4870 (2021).
  - [18] X. Xie, K. A. Persson, and D. W. Small, *Journal of Chemical Theory and Computation* **16**, 4256 (2020), pMID: 32502350.

- [19] L. D. Jacobson, J. M. Stevenson, F. Ramezanghorbani, D. Ghoreishi, K. Leswing, E. D. Harder, and R. Abel, *Journal of Chemical Theory and Computation* **18**, 2354 (2022), pMID: 35290063.
- [20] C. G. Staacke, S. Wengert, C. Kunkel, G. Csányi, K. Reuter, and J. T. Margraf, *Mach. Learn. Sci. Techn.* **3**, 015032 (2022).
- [21] D. Anstine, R. Zubatyuk, and O. Isayev, ChemRxiv 10.26434/chemrxiv-2023-296ch-v2 (2023).
- [22] D. P. Metcalf, A. Jiang, S. A. Spronk, D. L. Cheney, and C. D. Sherrill, *Journal of Chemical Information and Modeling* **61**, 115 (2021).
- [23] F. L. Hirshfeld, *Theoretica chimica acta* **44**, 129 (1977).
- [24] J. Čížek, *The Journal of Chemical Physics* **45**, 4256 (1966).
- [25] J. Paldus, J. Čížek, and I. Shavitt, *Phys. Rev. A* **5**, 50 (1972).
- [26] K. R. Bryenton, A. A. Adeleke, S. G. Dale, and E. R. Johnson, *WIREs Computational Molecular Science* **13**, e1631 (2023).
- [27] J. P. Perdew and A. Zunger, *Phys. Rev. B* **23**, 5048 (1981).
- [28] A. Ruzsinszky, J. P. Perdew, G. I. Csonka, O. A. Vydrov, and G. E. Scuseria, *The Journal of Chemical Physics* **125**, 194112 (2006), <https://pubs.aip.org/aip/jcp/article-pdf/doi/10.1063/1.2387954/15391310/194112.1.online.pdf>.
- [29] D. Hait and M. Head-Gordon, *The Journal of Physical Chemistry Letters* **9**, 6280 (2018).
- [30] M. G. Medvedev, I. S. Bushmarinov, J. Sun, J. P. Perdew, and K. A. Lyssenko, *Science* **355**, 49 (2017).
- [31] A. D. Kaplan, C. Shahi, P. Bhetwal, R. K. Sah, and J. P. Perdew, *Journal of Chemical Theory and Computation* **19**, 532 (2023), pMID: 36599075.
- [32] Y. Tawada, T. Tsuneda, S. Yanagisawa, T. Yanai, and K. Hirao, *The Journal of Chemical Physics* **120**, 8425 (2004).
- [33] S. Laricchia, E. Fabiano, and F. D. Sala, *The Journal of Chemical Physics* **138**, 124112 (2013).
- [34] D. R. Lonsdale and L. Goerigk, *Phys. Chem. Chem. Phys.* **22**, 15805 (2020).
- [35] X. Zheng, C. Li, D. Zhang, and W. Yang, *Science China Chemistry* **58**, 1825 (2015).
- [36] Q. Sun, T. C. Berkelbach, N. S. Blunt, G. H. Booth, S. Guo, Z. Li, J. Liu, J. D. McClain, E. R. Sayfutyarova, S. Sharma, S. Wouters, and G. K.-L. Chan, *WIREs Computational Molecular Science* **8**, e1340 (2018).
- [37] F. Jensen, *The Journal of Chemical Physics* **115**, 9113 (2001).
- [38] J. Dunning, Thom H., *The Journal of Chemical Physics* **90**, 1007 (1989).
- [39] E. R. Davidson and S. Chakravorty, *Theoretica chimica acta* **83**, 319 (1992).
- [40] N. Artrith, T. Morawietz, and J. Behler, *Phys. Rev. B* **83**, 153101 (2011).
- [41] P. Wind, M. Bjørge, A. Brakestad, G. A. Gerez S., S. R. Jensen, R. D. R. Eikås, and L. Frediani, *Journal of Chemical Theory and Computation* **19**, 137 (2023).
- [42] M. Gubler, J. A. Finkler, S. R. Jensen, S. Goedecker, and L. Frediani, *Noise tolerant force calculations in density functional theory: A surface integral approach for wavelet-based methods* (2024), arXiv:2410.02299 [physics.chem-ph].
- [43] B. K. Alpert, *SIAM Journal on Mathematical Analysis* **24**, 246 (1993).
- [44] B. Alpert, G. Beylkin, D. Gines, and L. Vozovoi, *Journal of Computational Physics* **182**, 149 (2002).
- [45] R. J. Harrison, G. I. Fann, T. Yanai, Z. Gan, and G. Beylkin, *The Journal of Chemical Physics* **121**, 11587 (2004), <https://pubs.aip.org/aip/jcp/article-pdf/121/23/11587/19247911/11587.1.online.pdf>.
- [46] T. Yanai, G. I. Fann, Z. Gan, R. J. Harrison, and G. Beylkin, *The Journal of Chemical Physics* **121**, 6680 (2004), <https://pubs.aip.org/aip/jcp/article-pdf/121/14/6680/19008023/6680.1.online.pdf>.
- [47] G. Beylkin and L. Monzón, *Applied and Computational Harmonic Analysis* **19**, 17 (2005).
- [48] J. P. Perdew, K. Burke, and M. Ernzerhof, *Phys. Rev. Lett.* **77**, 3865 (1996).
- [49] X. Gonze, B. Amadon, G. Antonius, F. Arnardi, L. Baguet, J.-M. Beuken, J. Bieder, F. Bottin, J. Bouchet, E. Bousquet, N. Brouwer, F. Bruneval, G. Brunin, T. Cavignac, J.-B. Charraud, W. Chen, M. Côté, S. Cottenier, J. Denier, G. Geneste, P. Ghosez, M. Giantomassi, Y. Gillet, O. Gingras, D. R. Hamann, G. Hautier, X. He, N. Helbig, N. Holzwarth, Y. Jia, F. Jollet, W. Lafargue-Dit-Hauret, K. Lejaeghere, M. A. Marques, A. Martin, C. Martins, H. P. Miranda, F. Naccarato, K. Persson, G. Petretto, V. Planes, Y. Pouillon, S. Prokhorenko, F. Ricci, G.-M. Rignanese, A. H. Romero, M. M. Schmitt, M. Torrent, M. J. van Setten, B. Van Troeye, M. J. Verstraete, G. Zerah, and J. W. Zwanziger, *Computer Physics Communications* **248**, 107042 (2020).
- [50] J. C. Slater, *Phys. Rev.* **81**, 385 (1951).
- [51] S. H. Vosko, L. Wilk, and M. Nusair, *Canadian Journal of Physics* **58**, 1200 (1980).
- [52] B. Hammer, L. B. Hansen, and J. K. Nørskov, *Phys. Rev. B* **59**, 7413 (1999).
- [53] A. D. Becke, *Phys. Rev. A* **38**, 3098 (1988).
- [54] C. Lee, W. Yang, and R. G. Parr, *Phys. Rev. B* **37**, 785 (1988).
- [55] A. D. Becke, *The Journal of Chemical Physics* **98**, 5648 (1993).
- [56] S. H. Vosko, L. Wilk, and M. Nusair, *Canadian Journal of physics* **58**, 1200 (1980).
- [57] P. J. Stephens, F. J. Devlin, C. F. Chabalowski, and M. J. Frisch, *The Journal of Physical Chemistry* **98**, 11623 (1994).
- [58] C. Adamo and V. Barone, *The Journal of Chemical Physics* **110**, 6158 (1999).
- [59] M. Ernzerhof and G. E. Scuseria, *The Journal of Chemical Physics* **110**, 5029 (1999).
- [60] J. Sun, A. Ruzsinszky, and J. P. Perdew, *Phys. Rev. Lett.* **115**, 036402 (2015).
- [61] A. P. Bartók and J. R. Yates, *The Journal of Chemical Physics* **150**, 161101 (2019).
- [62] J. W. Furness, A. D. Kaplan, J. Ning, J. P. Perdew, and J. Sun, *The Journal of Physical Chemistry Letters* **11**, 8208 (2020), pMID: 32876454.
- [63] K. Hui and J.-D. Chai, *The Journal of Chemical Physics* **144**, 044114 (2016).
- [64] T. Yanai, D. P. Tew, and N. C. Handy, *Chemical Physics Letters* **393**, 51 (2004).
- [65] J.-D. Chai and M. Head-Gordon, *The Journal of Chemical Physics* **128**, 084106 (2008).
- [66] N. Mardirossian and M. Head-Gordon, *Phys. Chem. Chem. Phys.* **16**, 9904 (2014).
- [67] S. Song, S. Vuckovic, E. Sim, and K. Burke, *Journal of Chemical Theory and Computation* **18**, 817 (2022), pMID:



35048707, <https://doi.org/10.1021/acs.jctc.1c01045>.